Original scientific paper

UDK 614.876:661.185
DOI 10.7251/COMEN2601001P

MXene-POLYURETHANE COMPOSITES AS WEARABLE STRAIN SENSORS FOR FINGER MOTION AND ON-SURFACE WRITING

Marija V. Pergal*, Ivan Pešić, Milena Rašljić Rafajilović,
Marko V. Bošković, Stefan D. Ilić, Marko Spasenović

Center for Microelectronic Technologies, Institute of Chemistry, Technology and Metallurgy, University of Belgrade, National Institute of the Republic of Serbia, Belgrade, Serbia

* Corresponding author: marija.pergal@ihtm.bg.ac.rs

Abstract: The remarkable applications of flexible and wearable sensors in human motion detection and health monitoring have attracted considerable attention from both academic and industrial communities. Wearable strain sensors for finger-motion monitoring demand materials that combine high conductivity, flexibility, long-term durability, fast response, and stable interfaces. Here we report a MXene–polyurethane (PU) platform built on an MDI/HBP/PDMS network with 50 wt% soft segments (PU-50) that serves as a biocompatible, elastic substrate for a $Ti_3C_2T_x$ conductive layer. MXene-PU composites were characterized by scanning electron microscopy (SEM), tensile testing and electrical measurements. SEM confirms the intended morphologies: layered, lamellar MXene stacks that form percolating pathways and a PU microphase-separated morphology between soft and hard segments. Three device variants were evaluated under finger flexion with increasing frequency: MXene on neat PU, PU with 1 wt% pure MXene in the bulk (PUMX), and PU with 1 wt% functionalized MXene (PEG-MXene) in the bulk (PUMP). Time-resolved resistance measurements acquired every 20 ms yielded clear, low-hysteresis $\Delta R/R_0$ waveforms across all frequencies, with a consistent performance hierarchy in which PUMP exhibited the lowest baseline drift and the most stable cycle-to-cycle response, while the neat PU device displayed the largest resistance modulation amplitude. On-surface drawing tests on the neat-PU-MXene sensor further demonstrated pattern-robust sensitivity, producing distinct, repeatable temporal signatures for triangle, circle, and square trajectories with rapid baseline recovery and minor residual offsets. The obtained results validate MXene–PU as a fast, stable, and comfortable candidate for wearable finger motion sensors. They also identify mild interface optimization—via functionalized MXene in the substrate—as an effective way to enhance signal stability and suppress baseline drift while preserving signal fidelity across frequencies. This motivates future work on long-term stability, environmental compensation, and integration with compact wireless readout for multi-gesture recognition.

Keywords: MXene, polyurethanes, tensile testing, wearable sensors, finger-motion sensing.

1. INTRODUCTION

Wearable strain sensors for human–motion tracking require materials that combine high electrical conductivity, mechanical compliance, fast response, and reliability. Two-dimensional transition-metal carbides/nitrides (MXenes, e.g., $Ti_3C_2T_x$) satisfy many of these constraints thanks to metallic-like conductivity, hydrophilicity enabling solution processing, and surface terminations (–O, –OH, –F) that facilitate interfacial bonding to polymers and tuning of piezoresistive response [1–4]. These features have propelled MXenes

to the forefront of flexible sensing, where recent reviews and studies document sensitive, low-hysteresis, and conformal motion sensors across joints and digits.

In parallel, MXenes and laser-induced graphene (LIG) have emerged as particularly attractive material families for wearable sensors: MXenes provide high electrical conductivity and facile deposition on compliant substrates [5], while LIG offers rapidly patternable, porous sp^2-carbon networks produced by direct laser induction with excellent conformability, low cost, and straightforward integration on polymers [6-9]. Taken together, these platforms enable skin-compatible devices that are lightweight, breathable, and mechanically resilient, supporting stable readouts during multiaxial deformation such as finger flexion. MXene films benefit from tunable surface chemistries for improved polymer adhesion and sensitivity [3], whereas LIG confers robust adhesion and microtextured interfaces that can suppress slippage and enhance signal fidelity under cyclic loading [10]. When combined with elastomeric polyurethane (PU) substrates, both MXene and LIG structures deliver fast response and repeatable signals suitable for continuous on-body monitoring, and their complementary processing routes (solution casting/spin coating/spray coating for MXenes and direct laser induction/transfer for LIG) open pathways toward scalable, application-specific sensor layouts.

A notable advantage of MXene strain sensors for finger-flexion monitoring is the ability to engineer microstructure/topography to achieve high gauge factors (GF), wide dynamic range, and application-relevant working windows. For example, topographic design of $Ti_3C_2T_x$ layers coupled with in-sensor machine learning enabled full-body avatar reconstruction with joint-motion fidelity from a sparse array of wearable modules—demonstrating both sensitivity and real-time edge processing [1]. Multilayered MXene structures further deliver precise gesture acquisition on multiple joints (neck, elbow, finger, knee, ankle), validating robustness to complex deformations [2]. Hybrid polymeric designs report very high GF (≈78–355) over large strain ranges (0–100%), sufficient for finger bending and other body movements [3]. Collectively, these studies underscore that MXene films can be tailored for high sensitivity without sacrificing usable strain range or response speed—key for finger flexion where frequencies of ~0.5–3 Hz are typical [1–3].

Beyond sensitivity, environmental stability and comfort are crucial. MXene surfaces are prone to oxidation and humidity-induced drift; thin PDMS encapsulation is a common mitigation that preserves signal quality while maintaining flexibility and skin comfort [11]. MXene-based textile and polymer composites also improve breathability and scalability to wearables (gloves/garments), with rapid responses (tens of milliseconds) suitable for real-time monitoring [11-13].

In parallel, substrate choice critically affects device durability, adhesion, and biocompatibility. Whereas polyimide (PI) is ubiquitous in lab prototypes, recent work highlights cross-linked PU networks as skin-safe, tunable, biocompatible and mechanically resilient platforms. PU films with ~50 wt% soft segments (PU-50) show favorable tensile behavior, transparency, non-cytotoxicity, good biocompatibility and—importantly—strong adhesion for transferred conductive LIG layer, leading to improved signal-to-noise ratio (SNR) in wearable sensors for biomedical and sport applications [7,10].

These findings motivate PU as a compliant support for conductive and biocompatible MXene films aimed at on-skin sensing, since the combination of elastic PU matrices and layered MXene structures enables excellent conformability and stable electromechanical coupling even under repetitive bending and twisting. Furthermore, good flexibility and high tensile strength of PU provide mechanical cushioning for the brittle MXene flakes, improving cyclic durability and preventing oxidative degradation, while the surface terminations of MXene (-O, -OH, -F) promote interfacial interactions with urethane groups, facilitating homogeneous dispersion and firm adhesion. As a result, MXene–PU composites offer a balanced platform that unites sensitivity, comfort, and excellent conductivity, making them ideal candidates for next-generation wearable strain sensors.

Within the polymer-MXene composites, our group have demonstrated (i) MXene-coated polymer (PVDF) membranes for heart-rate sensing with process-simple vacuum filtration and PDMS protection because PVDF is not biocompatible material and can not be use directly on the skin, and (ii) MXene-based finger-flex sensors with PVDF substrate benchmarked on index-finger motion using both laboratory SMUs and compact readout electronics. Both device lines show clean periodic waveforms during flexion–

extension and accurate timing extraction, indicating stable piezoresistive behavior compatible with lightweight electronics [6,14].

Against this backdrop, the present work targets a biocompatible and flexible MXene–PU platform tailored for finger-flexion sensing. Specifically, we synthesize cross-linked PU using MDI/HBP/PDMS chemistry and employ a PU-50 formulation with 50 wt.% soft PDMS segments as an elastic, skin-friendly substrate; deposit a $Ti_3C_2T_x$ film from isopropyl alcohol (IPA) dispersion to form the conductive layer; and evaluate the electrical response with sub-20 ms sampling using a Keysight 34461A under controlled strain protocols. Our aim is to combine strong PU–MXene interfacial adhesion and compliant PU mechanics with MXene's high conductivity and sensitivity to realize a conformal sensor with high signal-to-noise ratio, stable performance under cyclic bending, and straightforward integration into compact readout systems.

In this work, we prepare novel biocompatible and flexible PU–MXene sensors for real-time monitoring of finger flexion with high sensitivity, and—to identify the optimal sensor—we systematically investigate the influence of MXene functionalization on sensor performance, building on our prior PU–LIG transfer/adhesion insights [7] and leveraging advances in MXene topology and multilayer structures for robust finger-motion tracking [1–4,15,16].

2. EXPERIMENTAL

Polyurethane (PU) synthesis. Polyurethane was synthesized from 4,4′-methylenediphenyl diisocyanate (MDI; Sigma-Aldrich), a hyperbranched polyester (HBP; Polymer Factory), and poly(dimethylsiloxane) (PDMS; ABCR). A two-step polymerization was performed in a four-neck flask under a continuous argon atmosphere using a solvent mixture of *N*-methyl-2-pyrrolidone (NMP) and tetrahydrofuran (THF) [17-19]. The resulting polymer mixture was poured into Teflon molds, dried in a forced-air oven, and subsequently cut into films of the desired geometry.

MXene preparation. MXenes were synthesized using the established MILD method [19,22]. Briefly, Ti_3AlC_2 MAX-phase powder was etched with a mixture of LiF and concentrated HCl, followed by repeated washing with deionized water. The resulting dispersion was subjected to sonication and centrifugation; the supernatant was collected and dried to remove residual moisture. The dried MXene powder was then redispersed in isopropyl alcohol (IPA) at a mass ratio of 1:10.

Sensor platform and MXene coating. For the strain-sensor platform, we used polyurethane containing 50 wt.% soft segments (PU-50). The conductive layer was constructed from a thin MXene film. The PU platform measured 2 cm (length) × 1 cm (width) with a thickness of 500 μm. For coating, a 10 wt.% MXene dispersion was prepared using IPA as the solvent. Thin MXene layers were applied to the PU platform by spin coating with a two-step program (first step: 500 rpm; second step: 3000 rpm). After each deposited layer, the composite material was treated at 50 °C for 30 min in a vacuum oven to evaporate the solvent. Ten layers of the MXene dispersion on the PU platform were found to be optimal with respect to the strain-sensor electrical characteristics.

Sheet-resistance tracking during deposition. Sheet resistance was measured after each coating step. The first four layers were not conductive, and sheet resistance could not be measured. After the fifth MXene layer, the film became conductive and sheet resistance was recorded. The sheet resistance for five MXene layers on the PU platform was 10.4 kΩ/sq. With additional MXene layers, sheet resistance decreased; ten MXene layers were optimal for our application, yielding a sheet resistance of 3.03 kΩ/sq.

Electrical measurements. Resistance measurements were carried out using a Keysight 34461A (Keysight, California) digital multimeter operating in DCR mode with a two-wire configuration. The instrument was controlled from a PC via a custom data-acquisition program written in Python. Resistance data were collected every 20 ms throughout the measurement period.

Characterization. SEM images were obtained by using FESEM Tescan MIRA 3 XMU electron microscope. The cross-sectional image of PU-MXene composite was performed by optical microscope using Olympus BX53M. The thickness of MXene layer and PU was measured using Olympus Steam basic software. Tensile testing was performed at room temperature with the Shimadzu EZ-LX universal testing instrument equipped with a 5 kN load cell. The machine resolution was ±0.5 % of the indicated value

(within 1/500 to 1/1 of load cell rated capacity), and crosshead position detection accuracy was 0.1%. The samples were cut according to the ISO 527 standard and tested at a 30 mm/min speed. All the samples were conditioned at room temperature and in a desiccator for 48 hours before measurements. Three identical samples were tested for each series.

3. RESULTS AND DISCUSSION

3.1. Microstructure and morphology (SEM)

In Figure 1, the MXene films display the expected layered and lamellar morphology, with micron-scale $Ti_3C_2T_x$ flakes assembling into few- to multilayer stacks and interflake junctions that enable electronically percolating pathways, with direct flake–flake contacts in pristine MXene and modified interflake interfaces in the functionalized MXene. Hence, in the functionalized MXene, the multilayered structure is preserved but appears less compact, with increased interlayer separation compared to the pristine film.

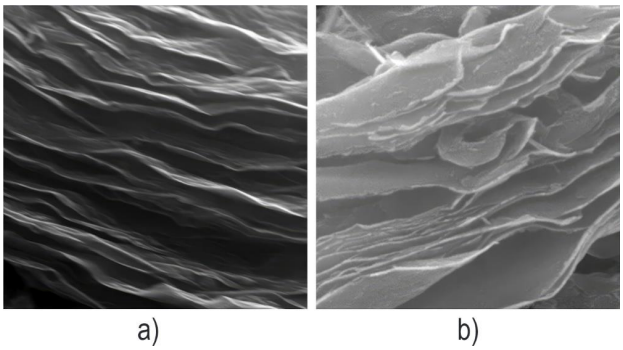

Figure 1. *SEM micrographs of a) pure MXene and b) functionalized MXene with PEG-silane (f-MXene).*

The accompanying SEM micrographs of pure PU, PUMX, and PUMP (Figure 2) show a pronounced microphase-separated structure in the pure PU matrix between PDMS-rich soft segments and MDI/HBP-derived hard domains, while the PUMX and PUMP samples additionally exhibit surface heterogeneities associated with the dispersed MXene fillers.

3.1.2. Optical microscopy

The optical micrograph of the PU–MXene composite cross-section (Figure 3) reveals a distinct bilayer structure, where the lower, darker region corresponds to the MXene coating and the upper, lighter region represents the PU substrate.

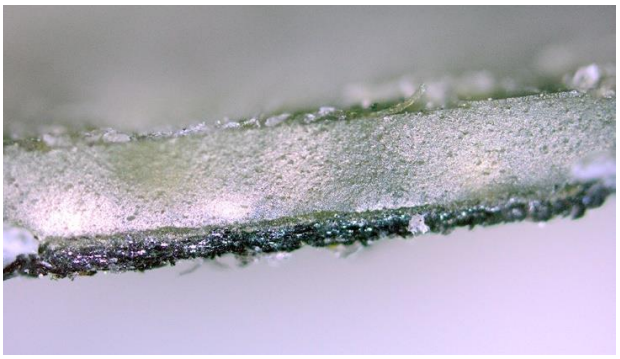

Figure 3. *Optical image of cross-sectional PU-MXene composite (100× magnification).*

The MXene layer appears continuous and well-adhered to the PU surface, forming a macroscopically continuous interface without obvious delamination or large cracks. This morphology suggests good interfacial contact between the conductive MXene layer and the elastic PU matrix, indicating the potential for efficient stress transfer and

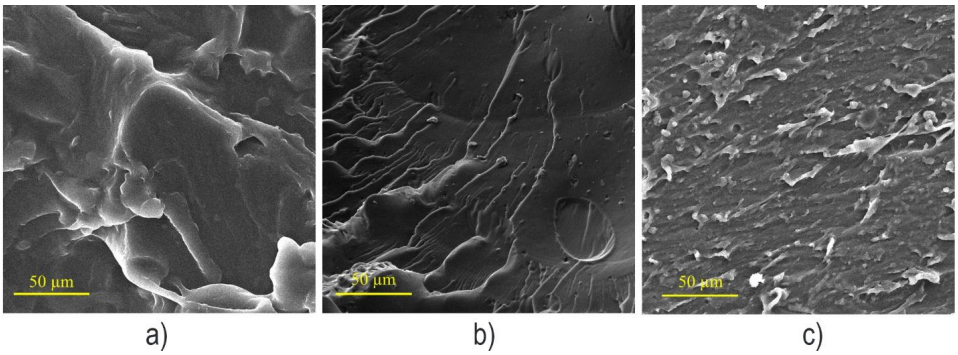

Figure 2. *SEM micrographs of a) pure PU; b) PUMX material (PU with dispersed 1 wt% pure MXene); c) PUMP (PU with dispersed 1 wt% f-MXene).*

stable electrical performance during bending or deformation. We measured the thickness of PU-MXene with an optical microscope (Figure 3), and we obtained a typical thickness of PU film of approximately 450 μm, and an apparent MXene-rich layer thickness of approximately 130 μm. The actual thickness of the MXene is smaller, as the apparent layer thickness is overestimated due to deformation during cutting/sectioning.

3.2. Mechanical properties

Across freestanding strips and PU-based composite films, the materials exhibited distinct mechanical responses depending on the presence and type of MXene filler (Table 1). The pure PU sample showed a low Young's modulus (0.98 MPa) and very high elongation at break (153.75%), characteristic of a soft and highly elastic elastomer suitable for conformal contact with curved skin surfaces. This flexibility enables easy bending and stretching without crack initiation or delamination of the conductive layer, maintaining comfort and adaptability when mounted on a finger.

Incorporation of 1 wt% pristine MXene (PUMX) significantly increased stiffness, with a Young's modulus of 83.56 MPa and a tensile strength of 11.44 MPa, while elongation at break decreased to 66.27%. This behavior indicates strong interfacial interactions between MXene sheets and the PU matrix, leading to more efficient load transfer but reduced extensibility. The reinforcement effect demonstrates that MXene sheets act as rigid nanofillers, effectively improving the composite's mechanical strength and dimensional stability during deformation, which is beneficial for preserving material integrity under cyclic strain.

Table 1. *Results of tensile testing of PU, PUMP and PUMX materials*

Material	Young's modulus, MPa	Tensile strength, MPa	Elongation at break, %
PU	0.975	0.681	153.75
PUMP	83.559	11.443	66.27
PUMX	14.540	6.080	101.26

The PU composite with 1 wt% pristine MXene (PUMX) showed an intermediate response, with a Young's modulus of 14.54 MPa, tensile strength of 6.08 MPa, and elongation at break of 101.26%. The moderate stiffness and improved stretchability compared to PUMP suggest that the absence of surface functionalization leads to partial MXene aggregation, resulting in intermediate stiffness and stretchability between pure PU and the functionalized-MXene composite. Such balanced mechanical properties are advantageous for strain-sensor applications, as they provide sufficient elasticity for large deformations together with improved mechanical strength for durability.

Overall, the mechanical results indicate that all three materials remain mechanically compliant enough for wearable strain-sensor applications, despite their markedly different stiffness levels. The PUMX composite offers an intermediate balance between elasticity and mechanical reinforcement, while PUMP provides maximum stiffness and PU retains the highest extensibility.

3.3. Finger-bending tests versus frequency: MXene on neat PU, PUMX, and PUMP

Figure 4 documents the physical configuration of the sensor during finger flexion, and Figure 5 presents the time-resolved resistance waveforms acquired under increasing flexion frequency for three materials—MXene on neat PU, PU with 1 wt% pristine MXene (PUMX), and PU with 1 wt% functionalized MXene (PUMP). All three devices generate clear, periodic $\Delta R/R_0$ signals that largely preserve their waveform morphology as frequency rises, particularly for the PUMP sensor.

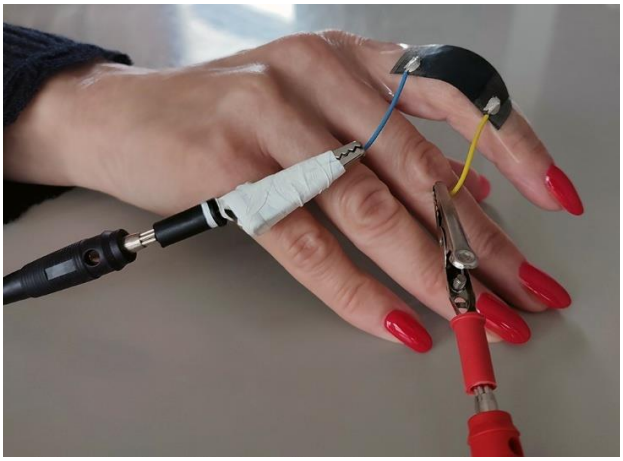

Figure 4. *Photograph of MXene sensor during finger flexion.*

Among the three, PUMP exhibits the cleanest peaks and troughs, the smallest baseline wander, whereas the MXene-on-neat-PU sensor exhibits the largest peak-to-peak amplitude. PUMX shows intermediate behavior, while the neat PU/MXene sensor exhibits a higher but less stable response with broader peaks and increased baseline drift. This hierarchy is attributed to improved interfacial coupling and more uniform stress transfer when functionalized flakes compatibilize the film–substrate interface.

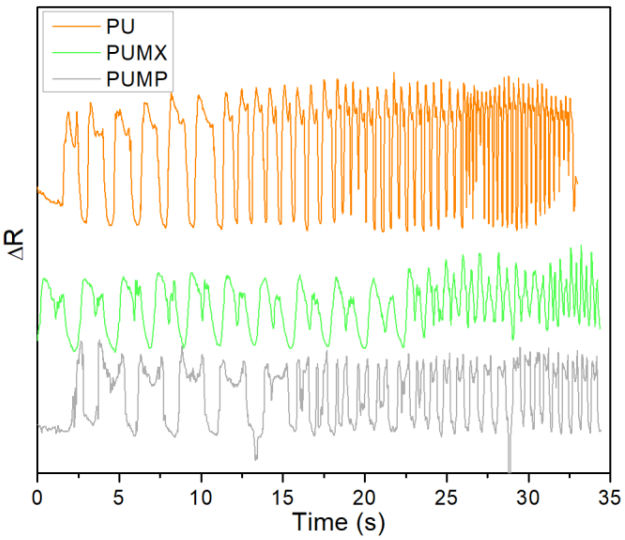

Figure 5. *Finger-bending results for the MXene-based sensor with increasing flexion frequency on: neat PU, PU with 1 wt% pristine MXene (PUMX), and PU with 1 wt% f-MXene (PUMP).*

Amplitude roll-off with increasing flexion frequency is minimal for the PUMP sensor, while the neat PU and PUMX devices show more pronounced waveform distortion at higher actuation rates; nevertheless, the phase lag remains small across all samples at the highest tested frequencies in Figure 5. Cycle-to-cycle comparisons indicate low hysteresis and stable percolation behavior, particularly for PUMP, whereas the neat-PU device exhibits modest drift consistent with weaker interfacial anchoring in the absence of embedded functionalized flakes.

From the plot, each periodic oscillation corresponds to one finger-bending cycle. The ΔR signal exhibits an increasing number of bending–releasing cycles over the 35 s interval, reflecting the progressive increase in flexion frequency during the measurement. The response time—the interval between the start of finger bending and the maximum ΔR value—is about 0.25–0.3 s, while the recovery time, corresponding to the return of ΔR to its baseline during finger extension, is roughly 0.3–0.35 s.

These results confirm that all three sensors (PU, PUMX, and PUMP) react rapidly and reproducibly to mechanical deformation. The PUMP sensor exhibits the most distinct and stable signal with minimal baseline drift, indicating efficient stress transfer and improved interfacial coupling between the functionalized MXene layer and the PU matrix. The PUMX signal is slightly less uniform, while the neat PU/MXene sensor shows a broader, higher-amplitude response accompanied by increased baseline drift and reduced signal stability, consistent with weaker interfacial coupling. Overall, the fast response and recovery times—both below one second—demonstrate that the MXene–PU sensors are well suited for real-time monitoring of dynamic finger movements.

From the plot, each ΔR fluctuation corresponds to a completed motion pattern (triangle, circle, or square). The ΔR signal reflects a sequence of repeated drawing gestures performed over a period of approximately 40 s, with each fluctuation corresponding to a distinct motion segment rather than a strictly periodic cycle. The response time, defined as the interval between the onset of motion and the peak ΔR signal, is approximately 0.3–0.4 s, while the recovery time—the return of ΔR to its baseline—is about 0.4–0.5 s.

These results confirm that the neat PU sensor maintains sensitivity and signal stability across different motion types during on-surface drawing tests. The ΔR amplitudes vary slightly depending on the shape: the triangle gesture produces sharper, higher-amplitude peaks due to abrupt directional changes, whereas the circle gesture shows smoother, more rounded waveforms associated with continuous motion. The square gesture exhibits intermediate behavior with consistent peak spacing. Overall, the consistent waveform profiles and rapid response/recovery times (<1 s) demonstrate that the MXene–PU sensor preserves sensitivity and signal fidelity across complex, multidirectional movements, confirming its suitability for real-time gesture differentiation and wearable human–motion tracking.

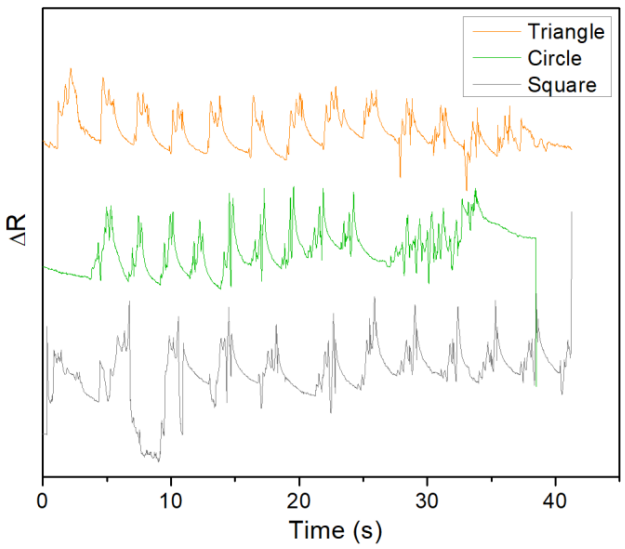

Figure 6. *Results of drawing a triangle, circle, and square on the MXene sensor made of neat PU.*

Among the three tested motion patterns—triangle, circle, and square— the triangle gesture produced the largest ΔR amplitude and the most pronounced response peaks and the sharpest response peaks in the recorded signal. This enhanced sensitivity arises from the abrupt directional changes inherent to the triangular motion, which are associated with stronger local strain variations and consequently larger resistance modulation in the MXene–PU sensing layer.

In contrast, the circle gesture produced smoother, lower-amplitude ΔR oscillations due to the continuous nature of the motion, while the square gesture exhibited intermediate sensitivity with distinct but less intense peaks. The results indicate that the sensor effectively captures both smooth and abrupt strain transitions, but its piezoresistive response is most pronounced during high-strain, discontinuous movements, confirming the sensor's strong responsiveness to rapid and angular deformations typical of the triangle-drawing motion.

3.4. On-surface pattern-drawing on the neat-PU sensor

Figure 6 presents the results of on-surface drawing tests performed directly on the neat-PU device, where triangle, circle, and square trajectories are traced. The sensor preserves sensitivity by producing distinct and reproducible temporal signatures—sharp ramps with acute turning-point spikes for the triangle, smooth quasi-sinusoidal modulation for the circle, and pronounced peaks with relatively abrupt transitions for the square. The peak-to-peak ΔR response varies systematically across shapes, with the triangle gesture producing the largest amplitudes, the circle yielding smoother and lower-amplitude waveforms, and the square exhibiting intermediate behavior. These observations indicate that the device transduces directional strain gradients reliably, retains a measurable response amplitude under changes in curvature and cornering, and recovers quickly with negligible residual offset. Consequently, shape changes do not extinguish the sensor response but remap it into distinctive, repeatable features suitable for gesture encoding and subsequent signal differentiation.

3.5. Overall interpretation and design rules

The combined evidence from Figure 2 and the device-level dynamics in Figures 4–6 indicates that interface optimization via a small content of functionalized MXene in the PU bulk strengthens stress transfer to the MXene film and suppresses drift. Preserving a layered, percolating network while ensuring strong adhesion to the microphase-separated PU prevents buckling or delamination under repetitive flexion. The ability in Figure 6 to track triangles, circles, and squares with consistent amplitude confirms pattern-robust sensitivity. Consequently, the PUMP configuration provides the most balanced combination of sensitivity, stability, and frequency-invariant response, with PUMX offering an improvement over neat PU and MXene on neat PU serving as a solid baseline. Altogether, these results support the central claim that MXene–PU platforms can deliver fast, robust, and gesture-resilient readouts for wearable finger-motion monitoring.

4. CONCLUSION

In this work, we combined a layered $Ti_3C_2T_x$ MXene film with a biocompatible, microphase-separated PU network to realize a conformal strain-sensor platform for finger-motion monitoring. SEM analysis confirmed the expected morphologies—lamellar MXene stacks forming percolating conductive pathways and PU domains exhibiting well-defined soft–

hard segment separation that provides both elasticity and mechanical stability.

Mechanical testing revealed that the introduction of pristine and functionalized MXene strongly influences stiffness and flexibility. The PUMP composite exhibited the most balanced behavior, combining enhanced modulus with adequate elongation, confirming efficient stress transfer and improved interfacial adhesion due to MXene functionalization.

Time-resolved electrical measurements collected at 20 ms intervals demonstrated clear, low-hysteresis $\Delta R/R_0$ responses over increasing bending frequencies for all three variants (MXene on neat PU, PUMX, and PUMP). Among them, PUMP showed the cleanest and most stable response with the lowest baseline drift, while the neat PU device exhibited the largest resistance modulation amplitude, validating that controlled interface optimization between the MXene layer and the PU substrate effectively improves signal stability and suppresses drift at higher actuation rates.

On-surface drawing experiments on the neat-PU sensor produced distinct and repeatable electrical signatures for triangle, circle, and square gestures, confirming that the device maintains pattern-robust sensitivity and rapid partial recovery with minor residual offsets even under complex strain fields. The triangle motion yielded the largest amplitude response, demonstrating the system's responsiveness to abrupt directional strain changes.

Taken together, these results validate MXene–PU composites as fast, stable, and comfortable platforms for wearable strain sensing, identifying PUMP as the most optimized configuration among the tested variants in terms of signal stability, repeatability, and drift suppression among the tested variants. Future research should address long-term MXene oxidation control and encapsulation, temperature and humidity compensation, extended cyclic durability, and standardized evaluation protocols for finger-flexion sensors. Integration with compact wireless modules and, in future studies, lightweight machine-learning algorithms will further advance these materials toward real-time gesture monitoring and soft-robotic control applications.

Acknowledgements. This research was supported by the Science Fund of the Republic of Serbia, #4950, Polymer/graphene heterostructures for physiological sensors – Polygraph. The authors would like to thank the Ministry of Science, Technological Development, and Innovation of Republic of Serbia (Contract No: 451-03-66/2025-03/200026). The results presented in this manuscript are in line with Sustainable Development Goal 3 (Good Health and Well-being) of the United Nations 2030 Agenda.

REFERENCES

[1] Yang, H.; Li, J.; Xiao, X.; *et al.* Topographic design in wearable MXene sensors with in-sensor machine learning for full-body avatar reconstruction. *Nat. Commun.* 2022, 13, 5311.

[2] Duan, S.; Lin, Y.; Wang, Z.; *et al.* Conductive porous MXene for bionic, wearable, and precise gesture motion sensors. *Research* 2021, 2021, 9861467.

[3] Leong, W.X.R.; Al-Dhahebi, A.M.; Ahmad, M.R.; Saheed, M.S.M. $Ti_3C_2T_x$ MXene–polymeric strain sensor with huge gauge factor for body movement detection. *Micromachines* 2022, 13, 1302.

[4] Li, Z.; *et al.* $Ti_3C_2T_x$ MXene-Based Flexible Piezoresistive Physical Sensors: A Review. *ACS Nano* 2022, 16, 1734–1758.

[5] Pešić, I.; Bošković, M.V.; Rašljić Rafajilović, M.; *et al.* Wearable heart rate sensor based on MXene-coated polymer membrane. Ic*ETRAN Conference* 2025, Čačak.

[6] Ilić, S. D. et al., Laser-Induced Graphene for Wearable Respiratory Monitoring," 2023 IEEE 33rd International Conference on Microelectronics (MIEL), Niš, Serbia, 2023, pp. 1–4

[7] Vojnović, V.; Spasenović, M.; Pešić, I.; *et al.* Pulse sensors based on laser-induced graphene transferred to biocompatible polyurethane networks: fabrication, transfer methods, characterization and application. *Chemosensors* 2025, 13, 122.

[8] Gavran, A et al. Laser-Induced Graphene on Biocompatible PDMS/PEG Composites for Limb Motion Sensing. *Sensors* 2025, 25, 5238.

[9] Vićentić, T. et al. Laser-Induced Graphene for Heartbeat Monitoring with HeartPy Analysis, *Sensors* 2022, 22, 6326.

[10] Barja, A.M.; Ryu, Y.K.; Tarancón, S.; Tejado, E.; Hamada, A.; Velasco, A.; Martinez, J. Laser-Induced Graphene Strain Sensors for Body

Movement Monitoring. *ACS Omega* 2024, 9, 38359.
[11] Lu, W.; *et al.* PDMS-Encapsulated MXene@ Polyester Fabric Strain Sensor with Humidity-Drift Suppression. *Nanomaterials* 2022, 12, 871.
[12] Chen, X.; *et al.* Flexible breathable MXene-textile pressure sensors with fast response. *npj Flex. Electron.* 2025, 9, 69.
[13] Kumar, P.; Sephra, P.; Gupta, M.; Jeoti, V.; Tharini, C.; Stojanović, G. M. Flexible and sustainable energy storage: Recent progress and prospects in wearable supercapacitors, *J. Energy Storage.* 2026, 141, 119173.
[14] Ilić, S.D.; Spasenović, M.; Pešić, I.; *et al.* MXene-Based Physical Sensor for Real-Time Monitoring of Finger Flexion. *MIEL* conference 2025.
[15] Yang, W.; *et al.* MXene-based flexible sensors for wearable applications (review). *Soft Sci.* 2025, 5, 33.
[16] Gao, Y.; et al. Thermo-Responsive Self-Recoverable Porous Sensors with Writable Electrodes: Advancing Wearable Motion Detection, *Adv. Sci.* 2025, e17254.
[17] Pergal, M.; et al. Poly (urethane-siloxane) s based on hyperbranched polyester as cross-linking agent: synthesis and characterization, *J. Serb. Chem. Soc.* 2012, 77, 919.
[18] Džunuzović, J.; et al. Synthesis and swelling behavior of polyurethane networks based on hyperbranched polymer, *Hem. Ind.* 2011, 65, 637.
[19] Pergal, M.; et al. Structural, thermal and surface characterization of thermoplastic polyurethanes based on poly(dimethylsiloxane), *J. Serb. Chem. Soc.* 2014, 79, 843.
[20] Balaban, M.; et al. The effect of polar solvents on the synthesis of poly(urethane–urea–siloxane)s, *J. Serb. Chem. Soc.* 2012, 77, 1457.
[21] Stefanović, I.; et al. Poly (urethane-dimethylsiloxane) copolymers displaying a range of soft segment contents, noncytotoxic chemistry, and nonadherent properties toward endothelial cells, *J. Biomed. Mater. Res. A*, 2015, 103, 1459.
[22] Pešić, I. et al. Synthesis and properties of *in situ* prepared polyurethane/PEG-MXene nanocomposites, *Prog. Org. Coat.* 2025, 203, 109158.

MXene–ПОЛИУРЕТАНСКИ КОМПОЗИТИ КАО НОСИВИ СЕНЗОРИ ДЕФОРМАЦИЈЕ ЗА ПОКРЕТЕ ПРСТИЈУ И ПИСАЊЕ ПО ПОВРШИНИ

Сажетак: Изузетне примене флексибилних и носивих сензора у детекцији људских покрета и праћењу здравља привукле су значајну пажњу академске и индустријске заједнице. Носиви сензори деформације за праћење покрета прстију захтевају материјале који комбинују високу проводљивост, флексибилност, дуготрајну издржљивост, брз одзив и стабилне интерфејсе. У овом раду представљамо MXene–полиуретан (PU) платформу засновану на MDI/HBP/PDMS мрежи са 50 мас.% меких сегмената (PU-50), која служи као биокомпатибилна, еластична подлога за проводни слој $Ti_3C_2T_x$. MXene-PU композити су карактерисани скенирајућом електронском микроскопијом (SEM), испитивањем на затезање и електричним мерењима. SEM потврђује очекиване морфологије: слојевите, ламеларне MXene структуре које формирају перколационе путеве, као и микрофазно раздвајање PU између меких и тврдих сегмената. Три варијанте уређаја испитиване су при савијању прста са растућом фреквенцијом: MXene на чистом PU, PU са 1 мас.% чистог MXene у запремини (PUMX) и PU са 1 мас.% функционализованог MXene (PEG-MXene) у запремини (PUMP). Временски разлучена мерења отпора, прикупљена сваких 20 ms, показала су јасне $\Delta R/R_0$ сигнале са малом хистерезом при свим фреквенцијама, уз доследну хијерархију перформанси у којој је PUMP показао најмањи помак базне линије и најстабилнији одзив из циклуса у циклус, док је уређај на чистом PU показао највећу амплитуду промене отпора. Испитивања цртања по површини на сензору MXene–PU додатно су показала робусну осетљивост на обрасце, генеришући јасне и поновљиве временске сигнале за путање троугла, круга и квадрата, уз брз

опоравак базне линије и мале преостале одступе. Добијени резултати потврђују да је MXene–PU брз, стабилан и удобан кандидат за носиве сензоре покрета прстију. Такође указују да блага оптимизација интерфејса – путем функционализованог MXene у подлози – представља ефикасан начин за побољшање стабилности сигнала и смањење помака базне линије, уз очување верности сигнала при различитим фреквенцијама. Ово отвара могућности за будућа истраживања дугорочне стабилности, компензације утицаја околине и интеграције са компактним бежичним системима очитавања за препознавање више гестова.

Кључне речи: MXene, полиуретани, испитивање на затезање, носиви сензори, детекција покрета прстију.

Paper received: 5 February 2026 **Paper accepted: 30 March 2026**